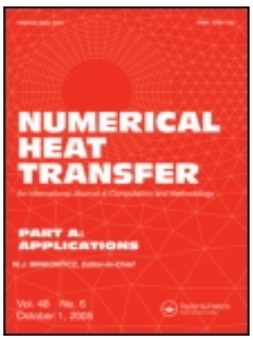

Taylor & Francis
Taylor & Francis Group

Numerical Heat Transfer, Part A: Applications
An International Journal of Computation and Methodology

ISSN: 1040-7782 (Print) 1521-0634 (Online) Journal homepage: http://www.tandfonline.com/loi/unht20

Numerical Simulation of Laminar Film Condensation in a Horizontal Minitube with and Without Non-Condensable Gas by the VOF Method

Zhan Yin, Yanling Guo, Bengt Sunden, Qiuwang Wang & Min Zeng

To cite this article: Zhan Yin, Yanling Guo, Bengt Sunden, Qiuwang Wang & Min Zeng (2015) Numerical Simulation of Laminar Film Condensation in a Horizontal Minitube with and Without Non-Condensable Gas by the VOF Method, Numerical Heat Transfer, Part A: Applications, 68:9, 958-977, DOI: 10.1080/10407782.2015.1023143

To link to this article: https://doi.org/10.1080/10407782.2015.1023143

Numerical Heat Transfer, Part A, 68: 958–977, 2015

ISSN: 1040-7782 print/1521-0634 online
DOI: 10.1080/10407782.2015.1023143

Taylor & Francis
Taylor & Francis Group

NUMERICAL SIMULATION OF LAMINAR FILM CONDENSATION IN A HORIZONTAL MINITUBE WITH AND WITHOUT NON-CONDENSABLE GAS BY THE VOF METHOD

Zhan Yin[1], Yanling Guo[1], Bengt Sunden[2], Qiuwang Wang[1], and Min Zeng[1]

[1]*Key Laboratory of Thermo-Fluid Science and Engineering, MOE, School of Energy and Power Engineering, Xi'an Jiaotong University, Xi'an, Shaanxi, P. R. China*

[2]*Division of Heat Transfer, Department of Energy Sciences, Lund University, Lund, Sweden*

Based on the volume of fluid (VOF) method, a steady three-dimensional numerical simulation of laminar film condensation of water vapor in a horizontal minitube, with and without non-condensable gas, has been conducted. A user-defined function defining the phase change is interpreted and the interface temperature is correspondingly assumed to be the saturation temperature. An annular flow pattern is to be expected according to a generally accepted flow regime map. The heat-transfer coefficient increases with higher saturation temperature and a smaller temperature difference between the saturation and wall temperatures, but varies little with different mass flux and degree of superheat. The existence of a non-condensable gas will lead to the generation of a gas layer between vapor and liquid, resulting in a lower mass-transfer rate near the interface and higher vapor quality at the outlet. In consequence, the heat-transfer coefficient of condensation with a non-condensable gas drops sharply compared with that of pure vapor condensation. Meanwhile, the non-condensable gas with a smaller thermal conductivity would cause a stronger negative effect on heat flux as a result of a higher thermal resistance of heat conduction in the non-condensable gas layer.

1. INTRODUCTION

When the vapor temperature is lower than the saturation temperature, condensation occurs on a cooling surface, during which the vapor phase is transferred to the liquid phase. Its high performance has been widely used during chemical processes and in the power industry, such as in turbine plants and the condenser in air conditioners. Because of the increasing demand for higher performance in compact devices, microchannel heat exchangers have received extensive attention

Received 28 October 2014; accepted 15 January 2015.

Address correspondence to Min Zeng, Key Laboratory of Thermo-Fluid Science and Engineering, Ministry of Education, Xi'an Jiaotong University, Xi'an, Shaanxi 710049, China. E-mail: zengmin@mail.xjtu.edu.cn

Color versions of one or more of the figures in the article can be found online at www.tandfonline.com/unht.

NOMENCLATURE

A, B	secondary parameter	T_{TD}	judging parameter of flow pattern
c_p	isobaric specific heat, J $(kgK)^{-1}$	$\vec{v}$	velocity, m s^{-1}
D	diameter of the minitube, m	W	mass fraction of non-condensable gas, %
F	surface tension, N	X	Martinelli parameter
F_{TD}	judging parameter of flow pattern	x, y, z	coordinate directions, m
f	secondary parameter	x'	vapor quality
G	mass flux, $kg(m^2s)^{-1}$	α	volume fraction, %
g	gravity, m s^{-2}	κ	interface curvature
h	heat-transfer coefficient, $W(m^2{\cdot}K)^{-1}$	μ	dynamic viscosity coefficient, $Pa{\cdot}s^{-1}$
j	superficial velocity, m s^{-1}	ρ	density, kg m^{-3}
K_{TD}	judging parameter of flow pattern	σ	surface tension coefficient, N m^{-1}
k	thermal conductivity, W $(m{\cdot}K)^{-1}$	φ	physical property
L	length of minitube, m	0	pure vapor condensation
L_H	latent heat of vapor, J kg^{-1}	i, j, q	index of phase
m	condensate mass flow rate, g s^{-1}	in	inlet
$\dot{\boldsymbol{m}}$	mass source due to phase change, kg $(m^3{\cdot}s)^{-1}$	inter	interface
		l	liquid phase
n	categories of phases	out	outlet
$\hat{\boldsymbol{n}}$	unit normal	S	saturation
p	pressure, Pa	v	vapor phase
q	heat flux, k W m^{-2}	w	wall
r	mass transfer coefficient, s^{-1}	CSF	continuum surface force
T	temperature, K	VOF	volume of fluid

in recent years, especially in the field of electronic applications. However, a non-condensable gas has a detrimental effect on condensation heat transfer. The presence of even a small quantity of non-condensable gas in the condensing vapor has a profound influence on the resistance to heat transfer in the region of the liquid–vapor interface [1]. Therefore, in order to design the appropriate heat-transfer equipment involving condensation, a fundamental understanding of the condensation of vapor with and without a non-condensable gas is necessary.

Nusselt [2] developed an analytical solution of a laminar film condensation of stagnant pure vapor on a vertical plate based on several basic assumptions, discovering the influence of saturation temperature, wall temperature, and physical properties on condensation heat transfer. The heat-transfer coefficient correlation can also be applied to condensation on a horizontal tube and sphere surface with minor revision. Based on Nusselt's research, Rohsenow and Hartnett [3] took into account a nonlinear temperature profile in the liquid film and made modifications on the energy balance, which includes the additional energy required to cool the film below the saturation temperature.

During the internal convective condensation process, the vapor and liquid are in simultaneous motion inside the channel; therefore, a complicated flow regime may exist in the multiphase flow. Mandhane et al. [4] and Taitel and Dukler [5] proposed flow regime maps for gas–liquid flow in horizontal or near-horizontal round tubes, including the stratified flow, annular flow, dispersed flow, and intermittent flow. Ganapathy et al. [6] developed a numerical model for the simulation of condensation heat transfer and fluid flow characteristics in a single microchannel based on the

volume of fluid (VOF) approach. The conventional governing equations of volume fraction and energy were modified to include source terms that account for mass transfer at the liquid–vapor interface and the associated release of latent heat. The two-phase frictional pressure drop and Nusselt number were validated with empirical correlations and a qualitative comparison of various flow patterns against experimental visualization data was conducted, acquiring a reasonable result. A simulation of condensation flow in a rectangular microchannel with the VOF method was also carried out by Chen et al. [7]. A thermal equilibrium model assuming that the interface temperature is at saturation was combined with the present VOF model. The numerical method was validated against experiments, and the simulation results predicted the flow pattern transition well. Wang et al. [8] presented a weighting correlation for a 1.46 mm rectangular multi-port aluminum condenser tube to account for all the flow regimes experienced from the flow visualizations. The final result can be applied for the design of a condenser with millimeter-scale tubes. Jassim et al. [9] studied the probabilistic two-phase flow map based on a flow-visualization technique using an illuminated, diffuse, striped background with a web camera. The adopted technique has an average time-fraction classification error of less than 0.01.

At high vapor velocities and moderate liquid flow rates, annular flow is observed for horizontal gas–liquid flow, where buoyancy effects may tend to thin the liquid film on the top portion of the tube wall and thicken it at the bottom under such a condition [10]. Nebuloni and Thome [11] presented a theoretical and numerical model to predict laminar annular film condensation heat transfer in mini- and micro-channels of different internal shapes. The model was based on a finite-volume formulation of the Navier–Stokes and energy equations, including unsteady terms, surface tension, axial shear stresses, gravitational forces, wall conduction, interphase mass transfer, and near-to-wall effects. The numerical results were validated by various benchmark solutions and available experimental data, whereas the deviation of heat-transfer data was less than 20%. Da Riva et al. [12, 13] performed a three-dimensional VOF simulation of annular film condensation inside a 1 mm horizontal minichannel. The liquid phase varied from laminar to turbulent for different cases, whereas the vapor phase was always turbulent. The heat-transfer coefficient thus computed was almost independent of mass flux and vapor quality under the assumption of the laminar condensate flow. The influence of mass flux could be observed only when turbulence in the condensate film was taken into account. Louahlia-Gualous and Asbik [14] provided a general model for annular film condensation of refrigerants R123, R134a, and their mixtures inside a miniature tube, analyzing the effects of tube diameter on the condensate film thickness, pressure, local axial velocity, average heat transfer coefficient, and the friction factor. The numerical results indicated that the condensation heat transfer was intensified, but the friction factor decreased, with a smaller tube diameter. The numerical model can also be applied to condensation in the presence of a non-condensable gas.

As a non-condensable gas has an extremely detrimental effect on condensation, much attention has been devoted to condensation in the presence of non-condensable gases. Among numerical simulations of condensation with non-condensable gas, the main approach is to solve the governing equations of each phase supplemented by some reasonable assumptions and empirical correlations. On the basis of the boundary layer theory, Tang et al. [15] discussed the distribution of velocity and

temperature in the boundary layers under different non-condensable mass fractions and sub-cooled temperature of the wall during condensation outside a horizontal tube. Even with a small mass concentration of the non-condensable gas in the bulk mixture, the reduction in the average heat-transfer coefficient was obvious. The influence of sub-cooled temperatures on condensation was different when the mass fraction of non-condensable gas varied from small to relatively large. Li [16] carried out a simultaneous simulation of flows involving multispecies and fluids of gas and liquid in separate channels in vertical cylindrical condensers, accounting for the turbulent flow of the gas mixture, the condenser wall, and the turbulent flow of the coolant in the annular channel. The results indicated that the axial velocity of the gas mixture at the interface between the gas mixture and the condensate film cannot be neglected for flows involving high water vapor content. A three-dimensional numerical model for the convection–condensation of mixture vapor in a tube with edgefold-twisted-tape inserts under transition flow was presented by Cui et al. [17]. The variation of condensation and convection heat transfer during condensation with non-condensable gas was analyzed. The result showed that non-condensable gas mainly affected the condensation heat transfer, whereas it was hardly relevant to convection heat transfer. The heat and mass transfer analogy, which is regarded as an effective way for the simulation of condensation with non-condensable gas, was employed by Caruso et al. [18] and Lee et al. [19] to explore the influence of non-condensable gas on condensation. The predictions of the theoretical model agreed well with their experimental results. Chantana and Kumar [20], and Su et al. [21] experimentally investigated the effect of non-condensable gases on steam condensation in and over a vertical tube, respectively. They both found that the heat-transfer coefficient of condensation with a non-condensable gas fell sharply when compared with that of pure vapor condensation, and developed new empirical correlations for corresponding conditions.

Applications of the condensation process in industries are currently under rapid growth; however, the studies discussed earlier indicate that the existing knowledge of the mechanism of condensation is insufficient and inconclusive. Therefore, the present study mainly focuses on annular laminar film condensation in a 1 mm horizontal minitube with and without non-condensable gas. The adopted VOF model with a user-defined function defining the phase change is implemented in the commercial package ANSYS FLUENT [22] to perform a steady-state three-dimensional numerical simulation. The phase-change model is convenient for implementation and has been validated. The influence of inlet velocity, wall temperature, saturation temperature, and superheat of vapor on pure vapor condensation has been discussed first. Then, the effects of non-condensable gas, including different inlet-volume fractions and species, are explored on the basis of pure vapor condensation, using the same multiphase and phase-change models.

2. NUMERICAL MODEL

The current three-dimensional steady numerical simulation is carried out in the horizontal minitube as shown in Figure 1, which is based on the VOF method combined with a phase-change model. The hydraulic diameter and length of the tube are 1 and 50 mm, respectively. As pure vapor or vapor with a non-condensable gas enters the inlet, under the driving force caused by the temperature difference between

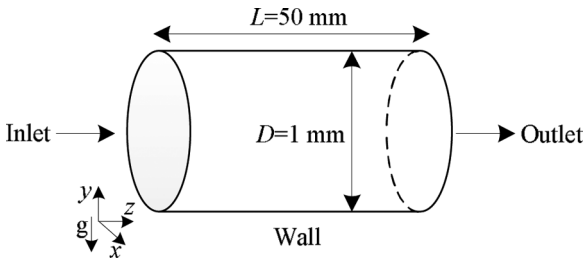

Figure 1. Physical model.

wall and saturation temperatures, condensation occurs. As a result, the multiphase flow consisting of vapor, liquid, and non-condensable gas leaves the outlet. The flow in each phase is laminar and incompressible. Under the present working parameters, the flow pattern in the minitube is assumed to be annular flow, namely, the liquid generated near the wall and vapor in the core are separated by the vapor–liquid interface, which will be examined in the latter part of this section. The working fluid along the interface is assumed to be saturated; therefore, the interface temperature is kept constant as the saturation temperature. The tendency of the liquid film to develop, the vapor quality, and the heat-transfer coefficient receive close attention in the present study.

2.1. VOF Method

There is substantial mass transfer and energy release near the interface boundary during condensation; therefore, the capture of the interface is of great importance during a numerical simulation of condensation. The VOF method is capable of computing multiphase flows of immiscible fluids without necessitating empirical closure laws to model the interaction between the phases, and effectively tracking the motion of the interface. A variable called the volume fraction of the phase in the computational cell is introduced for each phase. In any control volume, the volume fractions of all phases sum up to unity. If the q^{th} phase's volume fraction in the cell is denoted as α_q, then $\sum \alpha_q = 1$ is valid, and there are three possible conditions:

a. $\alpha_q = 0$: the cell is empty of the qth fluid.
b. $\alpha_q = 1$: the cell is full of the qth fluid.
c. $0 < \alpha_q < 1$: the cell contains the interface between the qth fluid and the other fluids.

Based on the local value of α_q, the appropriate properties and variables will be assigned to each control volume within the domain in the following way:

$$\varphi = \sum_{1}^{n} \alpha_q \varphi_q \text{ with } \varphi = \rho, k, \mu \tag{1}$$

$$\varphi = \frac{1}{\rho} \sum_{1}^{n} \alpha_q \rho_q \varphi_q \text{ with } \varphi = c_p \tag{2}$$

where $n = 2$ or 3, representing the categories of phases.

The tracking of the interfaces between the phases is accomplished by the solution of a continuity equation for the volume fraction of one or more phases. For the q^{th} phase, this equation has the following form:

$$\nabla \cdot \left(\alpha_q \rho_q \vec{v}_q\right) = \dot{m} \tag{3}$$

where $\dot{m}$ represents the mass source due to phase change. It is important to note that, in the VOF model, one phase will be designated as the primary phase, and the other phases are set as the secondary phases. The continuity equation of the secondary phase is solved to obtain the corresponding volume fraction, whereas the volume fraction of the primary phase is achieved based on the fact that volume fractions of all phases sum up to unity. In the present study, the vapor phase is assigned to be the primary phase for both condensation with and without non-condensable gas, which has been proved to be beneficial for numerical convergence.

In the VOF model, a single momentum equation is solved throughout the domain, and the resulting velocity field is shared among the phases. The three-dimensional steady Navier–Stokes equation is solved for momentum in the cells:

$$\nabla \cdot (\rho \vec{v}\vec{v}) = -\nabla p + \nabla \cdot \left[\mu\left(\nabla \vec{v} + \nabla \vec{v}^{\mathrm{T}}\right)\right] + \rho \vec{g} + \vec{F} \tag{4}$$

where $\vec{F}$ represents the surface tension, which will be discussed later.

The energy equation also shared among the phases is shown as followed:

$$\nabla \cdot \left(\vec{v}\left(\rho c_p T + p\right)\right) = \nabla \cdot (k \nabla T) + L_{\mathrm{H}} \dot{m} \tag{5}$$

where L_{H} represents the latent heat of vapor under consideration.

The Continuum Surface Force (CSF) model proposed by Brackbill et al. [23] has been implemented in the current VOF method, so that the addition of surface tension to the VOF calculation results in a source term in the momentum equation. The surface tension can be written in terms of the pressure jump across the surface while being expressed as a volume force using the divergence theorem. This volume force is added to the momentum equation in the following form:

$$F = \sum_{ij, i<j} \sigma_{ij} \frac{\alpha_i \rho_i \kappa_j \nabla \alpha_j + \alpha_j \rho_j \kappa_i \nabla \alpha_i}{0.5(\rho_i + \rho_j)} \tag{6}$$

where κ, the interface curvature, is defined in terms of the divergence of the unit normal:

$$\kappa = \nabla \cdot \hat{n} = \nabla \cdot \frac{\nabla \alpha_q}{\left|\nabla \alpha_q\right|} \tag{7}$$

Equation (6) allows for a smooth superposition of forces near cells where more than two phases are present. However, according to a test involving surface tension, the difference in the overall heat transfer is less than 5%; therefore, the influence of surface tension is neglected in this study.

2.2. Phase Change Model

As the standard VOF method does not cover the phase change, researchers have explored different ways to determine the mass and heat transfers during condensation [6, 7, 12, 13, 24–28]. Among these phase change models, a relatively simple and efficient method described below has been employed:

$$\dot{m} = -r\alpha_l\rho_l(T - T_s)/T_s, T \geq T_s \tag{8}$$

$$\dot{m} = r\alpha_v\rho_v(T_s - T)/T_s, T \leq T_s \tag{9}$$

where $\dot{m}$ is the source term in Eqs. (3) and (5), subscripts l and v indicate liquid and vapor respectively, r is a positive mass-transfer coefficient that will be discussed further, the unit of which is s^{-1}. There is no mass transfer between non-condensable gas and other phases.

From the above two equations, it can be noted that, when the cell temperature is higher than the saturation temperature, the source term will be negative, and when the cell temperature is lower than the saturation temperature, the source term will be positive, standing for the evaporation and condensation processes, respectively, for each condition. It can also be found obviously that the value of r has a close relationship with the mass- and heat-transfer rate. Therefore, the evaluation of r is a crucial matter. However, an agreement on the evaluation of r has not been reached as yet. This value differs from 5×10^3 to $5 \times 10^6\ s^{-1}$ for different working conditions, working fluids, and geometries [7, 12, 13, 26]. For a certain problem, an excessively large r will cause a numerical divergence problem, whereas a too small value will lead to significant difference between the interfacial and saturation temperatures, and both these cases lead to unreasonable solutions. In the present simulation, the effects of r on the interface temperature and wall heat flux are first checked, as depicted in Figure 2. It is obvious that, in the semi-logarithmic coordinate, the interface temperature increases almost linearly with the increasing mass-transfer coefficient, whereas the curve of the total heat flux on the wall versus the mass-transfer coefficient has a

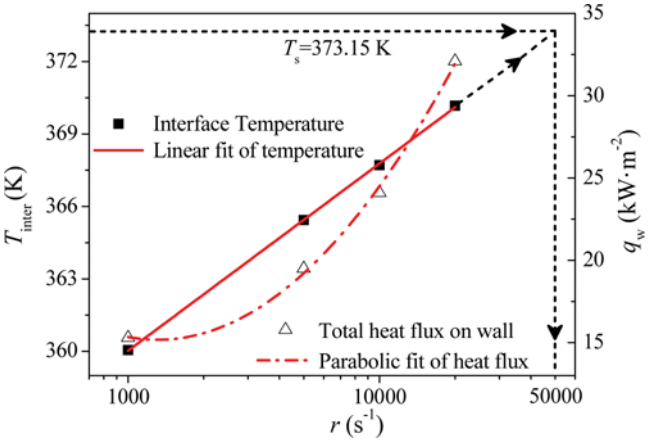

Figure 2. The evaluation of the mass-transfer coefficient.

nearly parabolic shape, the slope of which is elevated with a greater coefficient. From this, it is clear that the total heat flux is sensitive to the mass-transfer coefficient, the adopted value of which is of great importance. Afterwards, a linear fitted curve of the interface temperature is created as follows:

$$T_{\text{inter}} = 336.78 + 7.75 \log_{10} r \tag{10}$$

Then, under the assumption that the interface temperature is the saturation temperature, which is 373.15 K under current working conditions, the value of the mass-transfer coefficient can be confirmed to be $5 \times 10^4\,\text{s}^{-1}$. Finally, the numerical simulation is performed with $r = 5 \times 10^4\,\text{s}^{-1}$, and the interface temperature obtained is approximately 0.5 K lower than the saturation temperature. This deviation is an inevitable and acceptable computational error of the present research, whereas a similar phenomenon was also found in the studies of Da Riva et al. [12, 13], which was approximately 1 K. The corresponding heat-transfer performance is to be verified further by an empirical correlation.

2.3. Verification

A single-phase simulation of vapor in the same structure has been performed prior to the simulation of condensation in order to obtain a fully developed solution for the vapor flow and to eliminate the entrance effect. The velocity distribution of the single-phase simulation is used to set the inlet boundary condition. A pressure boundary condition is imposed at the outlet. The operating condition is 1 atm; therefore, the saturation temperature of water vapor is 373.15 K, while the wall is held isothermal at a uniform temperature. The pressure–velocity coupling algorithm adopted is SIMPLEC, while the PRESTO! (PREssureSTaggering Option) scheme is used in the simulation of the pressure interpolation. The QUICK scheme is used for the momentum, VOF, and energy equations.

First of all, a mesh-independence test of the numerical simulation in the physical model is carried out. In order to capture the vapor–liquid interface, the mesh size in the near wall region, where the liquid film is generated, is much finer than that in the vapor core region. Meanwhile, the mesh size is relatively coarser in the axial direction than in the radial direction in order to reduce the mesh number and to accelerate the numerical simulation. In total, seven sets of meshes displaying different number of cells are checked, and the results are shown in Figure 3. It is found that a finer mesh in the radial direction is more important, and the difference in terms of the total heat flux on the wall between the last two meshes is 1.14%. As a result, the mesh of 1.54×10^6 hexahedral cells is selected.

Then, the assumption of annular flow will be verified. According to a flow regime map for horizontal co-current gas–liquid flow shown in Figure 4 [5], the detailed flow pattern depends on several parameters that are based on the working parameter. The horizontal coordinate in the map is the Martinelli parameter X defined as follows:

$$X = \left[\frac{(\mathrm{d}p/\mathrm{d}z)_{\text{l}}}{(\mathrm{d}p/\mathrm{d}z)_{\text{v}}}\right]^{1/2} \tag{11}$$

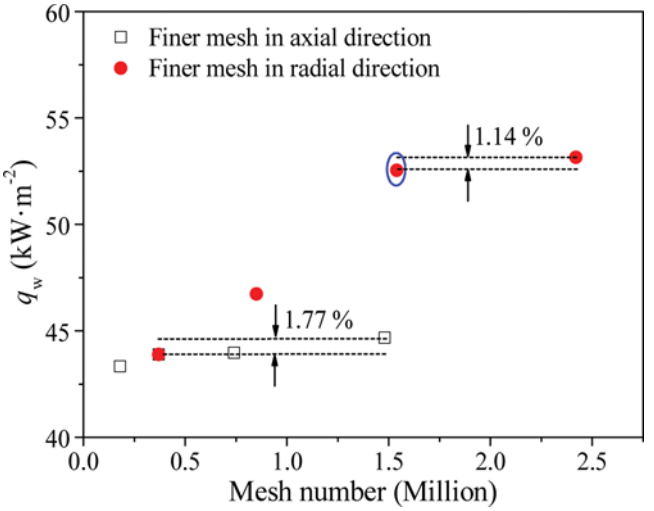

Figure 3. Mesh-independence test.

where $(dp/dz)_l$ and $(dp/dz)_v$ are, respectively, the frictional pressure gradients for the liquid and vapor phases flowing alone in the pipe, and they can be calculated as:

$$(dp/dz)_l = -\frac{2f_l G^2(1-x')^2}{\rho_l D} \tag{12}$$

$$(dp/dz)_v = -\frac{2f_v G^2 x'^2}{\rho_v D} \tag{13}$$

$$f_l = BRe_l^{-A}, Re_l = \frac{G(1-x')D}{\mu_l} \tag{14}$$

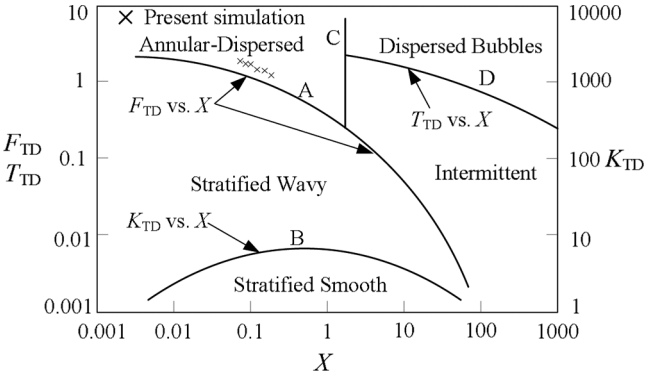

Figure 4. Flow regime map for the horizontal co-current gas–liquid flow.

$$f_v = BRe_v^{-A}, Re_v = \frac{Gx'D}{\mu_v} \tag{15}$$

In Eqs. (13) and (14), for laminar flow in round tubes, $B = 16$ and $m = 1$. The vertical coordinate differs from the specific flow transition, as for the wavy-annular and wavy-intermittent transitions depicted as curve A for the horizontal tube. It is calculated as:

$$F_{TD} = \left[\frac{\rho_v j_v^2}{(\rho_l - \rho_v)Dg}\right]^{0.5} \tag{16}$$

where j_v is the superficial gas velocity.

In the present case, it can be found from Figure 4 that the selected points along the tube during condensation are all in the annular-dispersed region. Therefore, the assumption of annular flow in the present research is proved to be correct.

3. RESULTS AND DISCUSSIONS

3.1. Pure Vapor Condensation

First, the influence of the inlet velocity and the wall temperature on condensation is explored. Figure 5 presents the development of the local heat-transfer coefficient along the axial direction. On one hand, the heat-transfer coefficient at different mass fluxes is almost the same. The same conclusion was drawn by Da Riva et al. [12] that, under the assumption of laminar condensate flow, the heat-transfer coefficient computed is found to be almost independent of mass flux and vapor quality. On the other hand, the heat-transfer coefficient at high wall temperature is relatively high. The variation of local vapor quality under different working parameters is also plotted in Figure 5. The outlet vapor quality is related to the vapor mass flux and

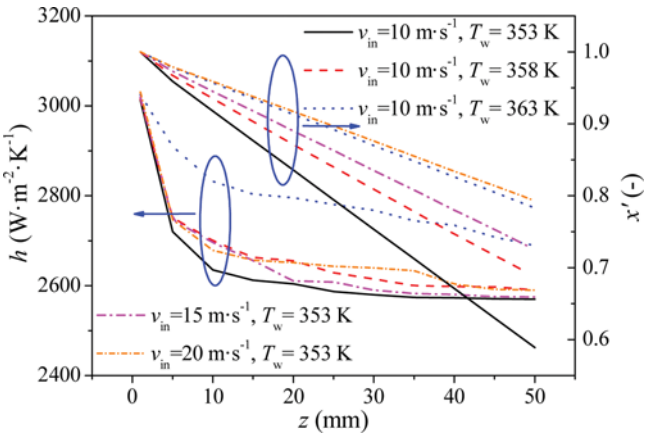

Figure 5. The influence of inlet velocity and wall temperature on the heat-transfer coefficient and vapor quality along the axial direction.

heat-transfer capacity. At the same mass flux, although a high wall temperature leads to a high heat-transfer coefficient, the difference between the saturation and wall temperatures declines more, the heat-transfer capacity falls, and then the outlet vapor quality is promoted as the wall temperature increases. At the same wall temperature and corresponding temperature difference, the heat-transfer capacity varies little with different mass flux, but a large amount of water vapor results in high vapor quality at the outlet.

Additionally, the effects of the saturation temperature of vapor on the heat-transfer performance are studied. The saturation temperature declines from 373 K to 343 K, whereas the inlet velocity remains at $10\,m\,s^{-1}$ and the difference between the saturation and wall temperatures varies from 5 K to 20 K. It can be distinguished from Figure 6 that the saturation temperature has a tremendous impact on the heat-transfer coefficient of condensation. Compared with a saturation temperature of 373 K, the average heat-transfer coefficient falls by 28.9%, 58.7%, and 84.1%, respectively, corresponding to saturation temperatures of 363 K, 353 K, and 343 K. It might be caused by a reduction of molecular activity and a relevant weakening of the phase interaction between vapor and liquid at a lower pressure and saturation temperature. In addition, the declination of heat-transfer coefficient slows down as the saturation and the wall temperatures decrease.

The above-mentioned research focuses on the condensation of saturated vapor; however, in industrial applications, vapor always enters the channel with a certain degree of superheat. Therefore, the following study is devoted to the condensation of superheated vapor. In Figure 7, it is apparent that the main difference in the temperature distribution during the condensation of saturated vapor and superheated vapor is in the vapor core, where there exists a large temperature gradient for the latter situation. The temperature of the superheated vapor that does not condense is reduced gradually to the saturation temperature, whereas that of the saturated vapor remains at the saturation temperature in the whole flow path. However, in the near

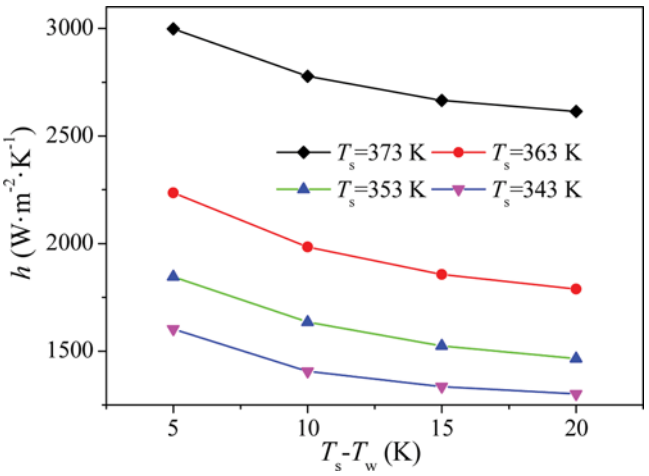

Figure 6. The influence of saturation temperature on the heat-transfer coefficient.

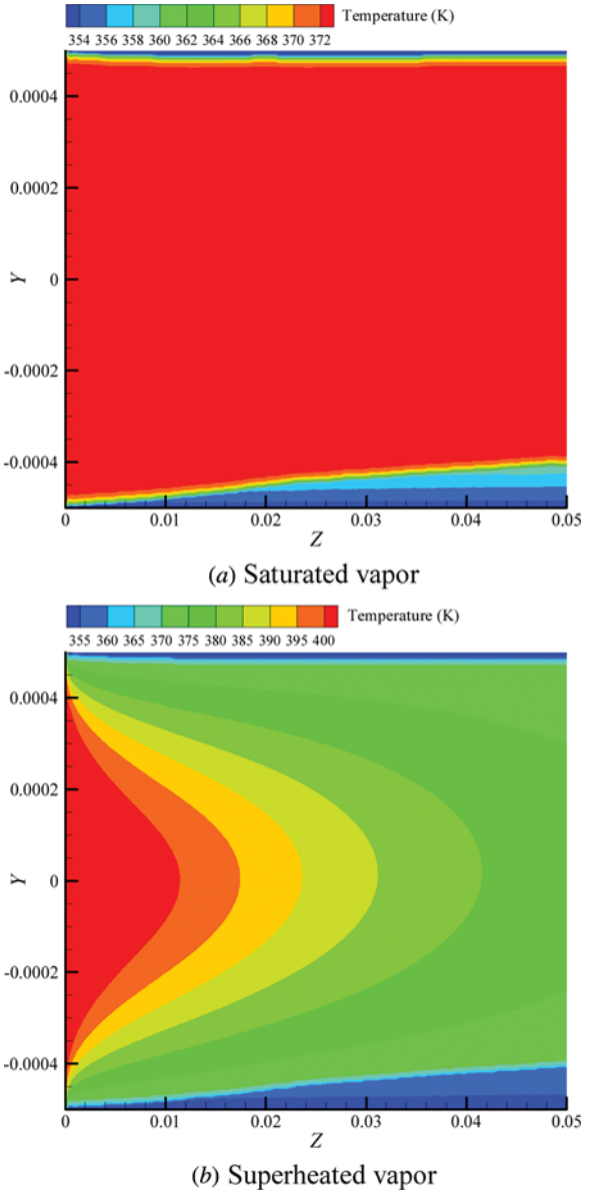

Figure 7. Temperature distribution at cross section $x = 0$ mm during condensation of saturated vapor (*a*) and superheated vapor (*b*).

wall region for both conditions, as soon as vapor is in contact with the cold wall and the temperature is reduced below the saturation temperature, the liquid film is generated in the same manner. The temperature distribution and thickness of the liquid film are alike; therefore, the average heat-transfer coefficients with different degrees of superheat is similar, as shown in Figure 8.

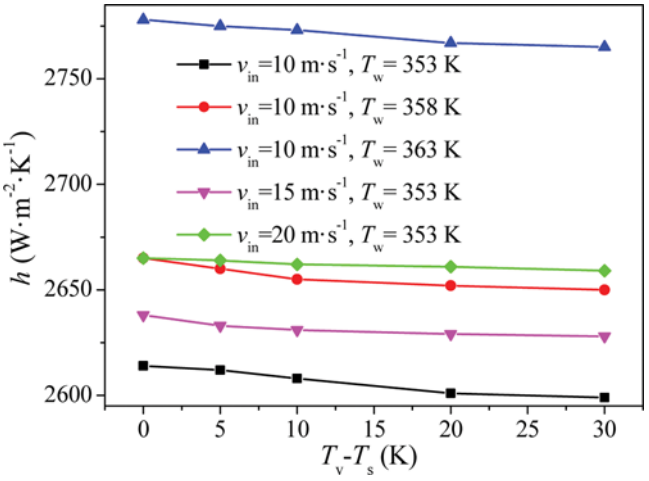

Figure 8. Average heat-transfer coefficient versus degree of superheat.

3.2. Condensation with Non-Condensable Gas

It is well known that when condensation is blended with a non-condensable gas, the existence of a gas layer will augment the resistance during the mass-transfer process. Air is first assigned as the non-condensable gas. In this study, the vapor–gas and gas–liquid interfaces are depicted in Figure 9, from which it is apparent that a non-condensable gas layer exists between the vapor in the core and the liquid near the wall. Before the water vapor arrives at the cold wall to condense, it has to pass through the gas layer by diffusion, which induces a negative effect on condensation. As a result, there is a sharp decline in the mass-transfer rate from vapor to liquid during condensation, as shown in Figure 10. Although the maximum values of the

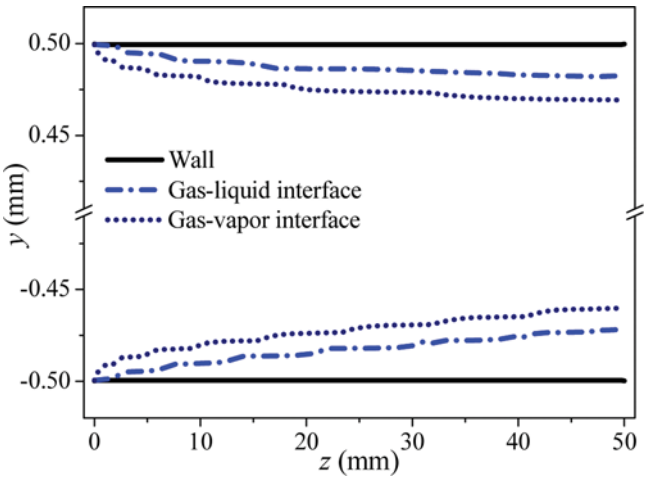

Figure 9. Vapor–gas interface and gas–liquid interface along the axial direction at cross section $x = 0$ mm.

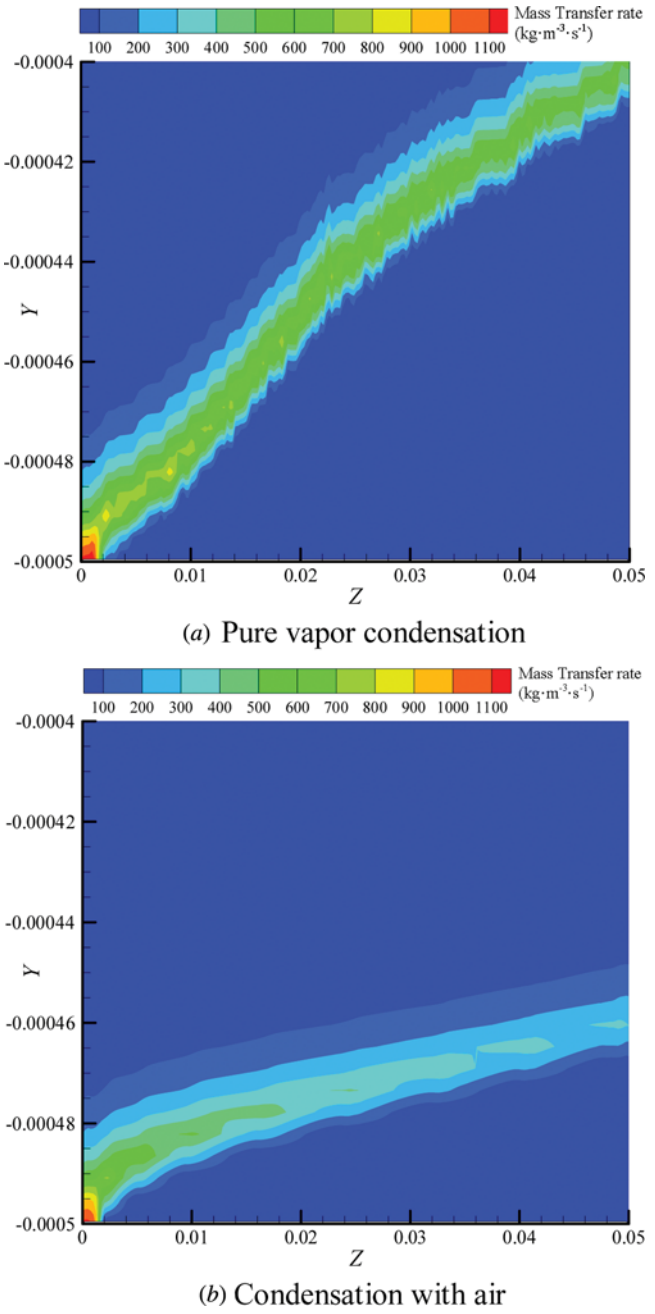

Figure 10. Mass-transfer rate of pure vapor condensation *(a)* and condensation with air *(b)* in the lower part of the tube at cross section $x = 0$ mm.

mass-transfer rate for both cases are almost the same, appearing at the inlet, the detail distribution near the liquid–vapor interface is quite different. Moving along the axial direction, the mass-transfer rate of the pure vapor condensation still keeps

a rather high value of approximately 700 kg m^{-3} s^{-1}. However, the mass-transfer rate of vapor condensation with non-condensable gas decreases drastically to approximately 300 kg m^{-3} s^{-1} till the outlet of the tube.

With the same inlet mass flux and low mass-transfer rate, the percentage of vapor that condenses will undoubtedly decline. As a consequence, the vapor quality at the outlet increases as the inlet volume fraction of air rises. The growth trend is sharper at first and slower toward the end, as depicted in Figure 11. In accordance with pure vapor condensation, the vapor quality at the outlet is raised with a higher inlet mass flux and wall temperature. With regard to the maximum inlet volume fraction of air, the vapor quality is improved by 22.1% on an average for all cases. As for the eventual condensate mass flow rate in Figure 12, it is decided by the combined action of mass flux and vapor quality. If only the wall temperature increases, the mass flux remains unchanged but the vapor quality increases, such that the condensate mass flow rate will decrease. However, if only the mass flux increases, the growth of the vapor quality is less than that of the inlet mass flux; therefore, the amount of condensate mass flow rate still ascends. Because condensation is severely blocked by the non-condensable gas, the heat-transfer coefficient of condensation with non-condensable gas declines severely. Figure 13 describes the average heat-transfer coefficient under different working conditions when the inlet volume fraction of air increases from 0.5% to 3%. Even a small air fraction (inlet volume fraction of 0.5%) will make the heat-transfer coefficient drop by 32.4%. However, as the inlet volume fraction of air increases to 3% gradually, the declining trend of the heat-transfer coefficient slows down, and it falls by 54.9% when the inlet volume fraction of air is 3%. The distinction of heat transfer under different working parameters is small, while the maximum and minimum deviation among cases is 13.8% and 5.7%, respectively.

What is important is that the existence of air will cause a reduction of the partial pressure of vapor and a corresponding lower saturation temperature. This leads to a weakness of the driving forces of condensation, namely, the temperature difference

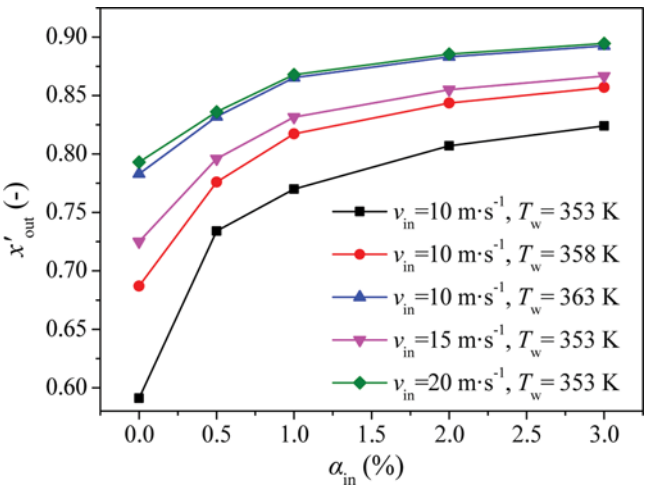

Figure 11. Vapor quality at the outlet as a function of the inlet volume fraction of air.

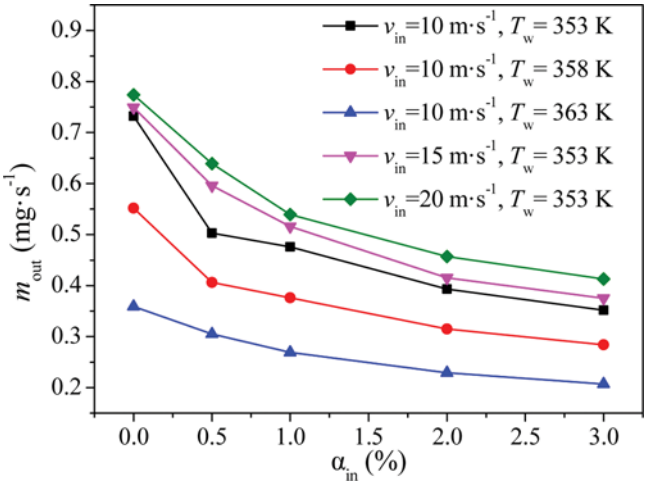

Figure 12. The effect of the inlet volume fraction of air on the condensate mass flow rate at the outlet.

between the wall temperature and the saturation temperature. However, in the present study, the maximum inlet volume fraction of air is 3%, and the air-inducing saturation temperature difference of vapor is less than 1 K. As a result, the effect of air on the saturation temperature of vapor can be ignored in this study.

As mentioned, vapor has to pass through the gas layer before it arrives at the cold wall to condense. Because the thermal conductivity of the non-condensable gas is much less than that of the liquid, the thermal conduction in the gas layer becomes the main thermal resistance during condensation with a non-condensable gas instead of thermal conduction in the liquid layer. Therefore, as can be seen in Figure 14, different non-condensable gases with different thermal conductivity give rise to

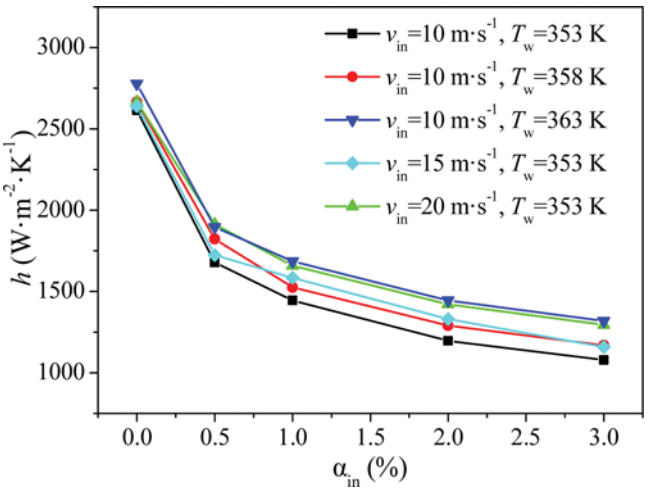

Figure 13. Heat-transfer coefficient at different inlet volume fractions of air.

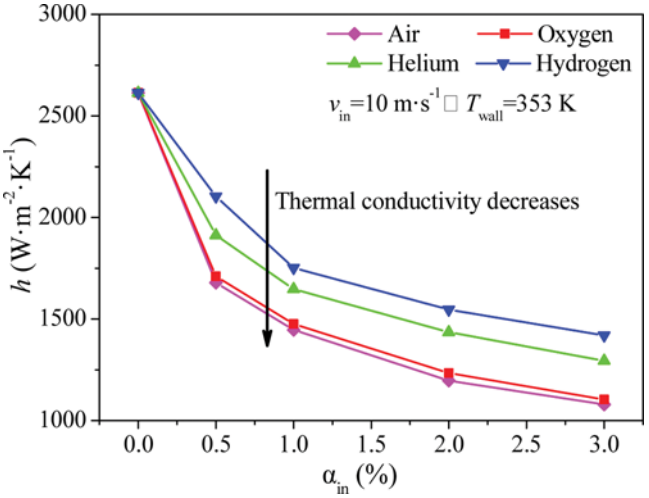

Figure 14. The effect of different non-condensable gases on the heat-transfer coefficient.

different heat-transfer performances. The thermal conductivity of hydrogen, helium, oxygen, and air decreases successively, and the heat-transfer coefficient of condensation with the same inlet volume fraction is demonstrated to descend in proper order. Compared with the heat-transfer coefficient of condensation with air, the average deviations of the heat-transfer coefficient of condensation with oxygen, helium, and hydrogen are 2.3%, 16.9%, and 26.8%, respectively.

In addition, a numerical simulation of laminar film condensation of water vapor with air on a vertical plate is also carried out in order to validate the numerical model applied for condensation with non-condensable gas, because studies on condensation

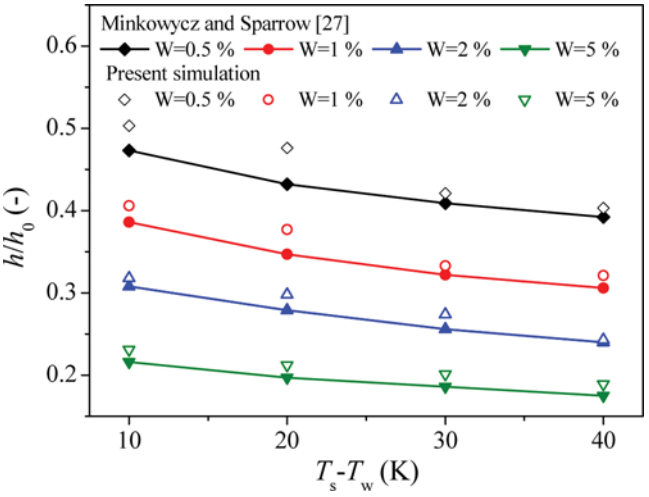

Figure 15. Condensation heat-transfer performance in the presence of air on an isothermal vertical plate.

inside horizontal minichannels in the presence of non-condensable gas are scarce. The results are compared with the analytical investigation of Minkowycz and Sparrow [29], the accuracy of which was verified by the experimental research of Slegers and Seban [30]. The effects of the temperature difference between the saturation and wall temperatures as well as the mass fraction of air on condensation are displayed in Figure 15. It can be found that the condensation heat-transfer coefficient decreases with a larger mass fraction of air and higher temperature difference. The average over-prediction is approximately 5.8%, indicating that the present method is capable of being applied to a numerical simulation of condensation with non-condensable gas.

4. CONCLUSIONS

In this article, a steady three-dimensional VOF numerical simulation of laminar film condensation of water vapor with and without a non-condensable gas inside a 1 mm horizontal minitube is carried out. The flow pattern is supposed to be annular flow and has been validated. The interface temperature is assumed to be the saturation temperature of vapor. The influence of inlet velocity, wall temperature, saturation temperature, and a degree of superheat is studied for pure vapor condensation. Air is, first, selected as the non-condensable gas and its inlet volume fraction varies from 0.5% to 3%. Then, the effect of various non-condensable gases on condensation is investigated. The following conclusions can be drawn from the present numerical simulations:

1. The heat-transfer coefficient of pure vapor condensation is nearly irrelevant with the inlet velocity and degree of superheat, but it will rise sharply with a higher saturation temperature and go up slightly with a smaller temperature difference between the saturation and the wall temperatures. The vapor quality declines almost linearly from the inlet till the outlet.
2. When condensation is blended with a non-condensable gas, the mass-transfer rate along the interface descends dramatically, resulting in higher vapor quality at the outlet and a sharp drop of the heat-transfer coefficient.
3. With the same working parameter, the non-condensable gas with a higher thermal conductivity will bring about a lesser reduction of the heat-transfer coefficient, because of a lower thermal resistance of heat conduction in the non-condensable gas layer.

ACKNOWLEDGMENTS

This present study was supported by the National Natural Science Foundation of China (Grant No. 51276139).

REFERENCES

1. J. G. Collier and J. R. Thome, *Convective Boiling and Condensation*, Oxford University Press, UK, 1994.
2. W. Nusselt, Die Oberflachenkondesation des Wasserdamffes the Surface Condensation of Water, *Zetrschr. Ver. Deutch. Ing.*, vol. 60, pp. 541–569, 1916.

3. W. M. Rohsenow and J. P. Hartnett, *Handbook of Heat Transfer*, McGraw-Hill, New York, 1973.
4. J. M. Mandhane, G. A. Gregory, and K. Aziz, A Flow Pattern Map for Gas-Liquid Flow in Horizontal Pipes, *Int. J. Multiphase Flow*, vol. 1, pp. 537–553, 1974.
5. Y. Taitel and A. E. Dukler, A Model for Predicting Flow Regime Transitions in Horizontal and Near Horizontal Gas-Liquid Flow, *AIChE J.*, vol. 22, pp. 47–55, 1976.
6. H. Ganapathy, A. Shooshtari, K. Choo, S. Dessiatoun, M. Alshehhi, and M. Ohadi, Volume of Fluid-based Numerical Modeling of Condensation Heat Transfer and Fluid Flow Characteristics in Microchannels, *Int. J. Heat Mass Transf.*, vol. 65, pp. 62–72, 2013.
7. S. H. Chen, Z. Yang, Y. Y. Duan, Y. Chen, and D. Wu, Simulation of Condensation Flow in a Rectangular Microchannel, *Chem. Eng. Process.: Process Intensif.*, vol. 76, pp. 60–69, 2014.
8. W. W. William Wang, T. D. Radcliff, and R. N. Christensen, A Condensation Heat Transfer Correlation for Millimeter-scale Tubing with Flow Regime Transition, *Exp. Thermal Fluid Sci.*, vol. 26, pp. 473–485, 2002.
9. E. W. Jassim, T. A. Newell, and J. C. Chato, Probabilistic Determination of Two-phase Flow Regimes in Horizontal Tubes Utilizing an Automated Image Recognition Technique, *Exp. Fluids*, vol. 42, pp. 563–573, 2007.
10. V. P. Carey, *Liquid-Vapor Phase-Change Phenomena*, Taylor & Francis Group, LLC, New York, 2008.
11. S. Nebuloni and J. R. Thome, Numerical Modeling of Laminar Annular Film Condensation for Different Channel Shapes, *Int. J. Heat Mass Transf.*, vol. 53, pp. 2615–2627, 2010.
12. E. Da Riva, D. Del Col, S. V. Garimella, and A. Cavallini, The Importance of Turbulence During Condensation in a Horizontal Circular Minichannel, *Int. J. Heat Mass Transf.*, vol. 55, pp. 3470–3481, 2012.
13. E. Da Riva and D. Del Col, Numerical Simulation of Laminar Liquid Film Condensation in a Horizontal Circular Minichannel, *J. Heat Transf.*, vol. 134, pp. 051019, 2012.
14. H. Louahlia-Gualous and M. Asbik, Numerical Modeling of Annular Film Condensation Inside a Miniature Tube, *Numer. Heat Transf., Part A: Appl.*, vol. 52, pp. 251–273, 2007.
15. G. H. Tang, H. W. Hu, Z. N. Zhuang, and W. Q. Tao, Film Condensation Heat Transfer on a Horizontal Tube in Presence of a Noncondensable Gas, *Appl. Therm. Eng.*, vol. 36, pp. 414–425, 2012.
16. J. D. Li, CFD Simulation of Water Vapour Condensation in the Presence of Non-condensable Gas in Vertical Cylindrical Condensers, *Int. J. Heat Mass Transf.*, vol. 57, pp. 708–721, 2013.
17. Y. Z. Cui, M. C. Tian, L. H. Zhang, G. P. Li, and J. B. Zhu, Three Dimensional Numerical Simulation of Convection-Condensation of Vapor with High Concentration Air in Tube with Inserts, *Chin. J. Chem. Eng.*, vol. 20, pp. 686–692, 2012.
18. G. Caruso and D. Vitale Di Maio, Heat and Mass Transfer Analogy Applied to Condensation in the Presence of Noncondensable Gases Inside Inclined Tubes, *Int. J. Heat Mass Transf.*, vol. 68, pp. 401–414, 2014.
19. K. Y. Lee and M. H. Kim, Effect of an Interfacial Shear Stress on Steam Condensation in the Presence of a Noncondensable Gas in a Vertical Tube, *Int. J. Heat Mass Transf.*, vol. 51, pp. 5333–5343, 2008.
20. C. Chantana and S. Kumar, Experimental and Theoretical Investigation of Air-steam Condensation in a Vertical Tube at Low Inlet Steam Fractions, *Appl. Therm. Eng.*, vol. 54, pp. 399–412, 2013.

21. J. Q. Su, Z. N. Sun, G. M. Fan, and M. Ding, Experimental Study of the Effect of Non-Condensable Gases on Steam Condensation Over a Vertical Tube External Surface, *Nucl. Eng. Des.*, vol. 262, pp. 201–208, 2013.
22. Ansys Fluent 12.0 Theory Guide, ANSYS Inc., USA, 2009.
23. J. U. Brackbill, D. B. Kothe, and C. Zemach, A Continuum Method for Modeling Surface Tension, *J. Comput. Phys.*, vol. 100, pp. 335–354, 1992.
24. Y. W. Zhang, A. Faghri, and M. B. Shafii, Capillary Blocking in Forced Convective Condensation in Horizontal Miniature Channels, *J. Heat Transf.*, vol. 123, pp. 501–511, 2001.
25. L. M. Pan, Z. W. Tan, D. Q. Chen, and L. C. Xue, Numerical Investigation of Vapor Bubble Condensation Characteristics of Subcooled Flow Boiling in Vertical Rectangular Channel, *Nucl. Eng. Des.*, vol. 248, pp. 126–136, 2012.
26. Z. Y. Liu, B. Sunden, and J. L. Yuan, VOF Modeling and Analysis of Filmwise Condensation Between Vertical Parallel Plates, *Heat Transf. Res.*, vol. 43, pp. 47–68, 2012.
27. Y. W. Zhang and A. Faghri, Numerical Simulation of Condensation on a Capillary Grooved Structure, *Numer. Heat Transf., Part A: Appl.*, vol. 39, pp. 227–243, 2001.
28. D. L. Sun, J. L. Xu, and Q. C. Chen, Modeling of the Evaporation and Condensation Phase-Change Problems with FLUENT, *Numer. Heat Transf., Part B: Fundam.*, vol. 66, pp. 326–342, 2014.
29. W. J. Minkowycz and E. M. Sparrow, Condensation Heat Transfer in the Presence of Noncondensables, Interfacial Resistance, Superheating, Variable Properties, and Diffusion, *Int. J. Heat Mass Transf.*, vol. 9, pp. 1125–1144, 1966.
30. L. Slegers and R. A. Seban, Laminar Film Condensation of Steam Containing Small Concentrations of Air, *Int. J. Heat Mass Transf.*, vol. 13, pp. 1941–1947, 1970.